INTERNATIONAL JOURNAL OF REMOTE SENSING
2023, VOL. 44, NO. 1, 59–77
https://doi.org/10.1080/01431161.2022.2157684

Taylor & Francis
Taylor & Francis Group

Inter-comparison of optical and SAR-based forest disturbance warning systems in the Amazon shows the potential of combined SAR-optical monitoring

Juan Doblas Prieto[a], Lucas Lima[b], Stephane Mermoz[c], Alexandre Bouvet[d], Johannes Reiche[e], Manabu Watanabe[f], Sidnei Sant Anna[a] and Yosio Shimabukuro[a]

[a]Earth Observation and Geoinformatics Division (DIOTG), National Institute for Space Research (INPE), São José dos Campos, Brazil; [b]SIG Formation, IDGEO, Toulouse, France; [c]GlobEO, Toulouse, France; [d]CNRS/CNES/IRD/INRAE/UPS, CESBIO, Toulouse, France; [e]Laboratory of Geo-information Science and Remote Sensing, Wageningen University, Wageningen, The Netherlands; [f]Earth Observation Research Center, Japan Aerospace Exploration Agency (JAXA), Chofu, Japan

ABSTRACT

More than half a decade after the launch of the Sentinel-1A C-band SAR satellite, several near real-time forest disturbances detection systems based on backscattering time series analysis have been developed and made operational. Every system has its own particular approach to change detection. Here, we have compared the performance of the main SAR-based near real-time operational forest disturbance detection systems produced by research agencies (INPE, in Brazil, CESBIO, in France, JAXA, in Japan, and Wageningen University, in the Netherlands), and compared them to the state-of-the-art optical algorithm, University of Maryland's GLAD-S2. We implemented an innovative validation protocol, specially conceived to encompass all the analysed systems, which measured every system's accuracy and detection speed in four different areas of the Amazon basin. The results indicated that, when parametrized equally, all the Sentinel-1 SAR methods outperformed the reference optical method in terms of sample-count F1-Score, having comparable results among them. The GLAD-S2 optical method showed superior results in terms of user's accuracy (UA), issuing no false detections, but had a lower producer accuracy (PA, 84.88%) when compared to the Sentinel-1 SAR-based systems (PA∼90%). Wageningen University's system, RADD, proved to be relatively faster, especially in heavily clouded regions, where RADD warnings were issued 41 days before optical ones, and the one that better performs on small disturbed patches (<0.25 ha) with a UA of 70.11%. Of all the high-resolution SAR methods, CESBIO's had the best results regarding UA (99.0%). Finally, we tested the potential of three hypothetical combined optical-SAR systems. The results show that these combined systems would have excellent detection capabilities, exceeding largely the producer's accuracy of all the tested methods at the cost of a slightly diminished user's accuracy, and constitute a promising and feasible approach for the forthcoming forest monitoring systems.

ARTICLE HISTORY
Received 23 May 2022
Accepted 6 December 2022

CONTACT Juan Doblas Prieto juan.doblas@inpe.br National Institute for Space Research (INPE), Sao Jose dos Campos, Brazil

POLICY HIGHLIGHTS

- Recently developed automated SAR-based tropical forest disturbance detection systems showed excellent detection accuracies, even in small, difficult-to-spot deforested patches.
- SAR detections can be as precise and as fast as optical ones, being more precise and faster in very cloudy areas or in areas subjected to illegal mining.
- The combination of recently developed SAR and optical warnings systems can yield optimized results, in terms of overall accuracy and producer's accuracy.

1. Introduction

Tropical forests constitute the biggest sink of global greenhouse gases (GHG), accounting for an annual removal of approximately 7.0 Gt CO_2e yr^{-1} (Harris et al. 2021). This leading role in GHG capture is threatened by deforestation, which is estimated to emit approximately 5.4 Gt CO_2e yr^{-1}. This figure represents double of the annual emissions associated with the removal of the remainder of the global forest formations (Harris et al. 2021). Although many initiatives have been implemented to reduce forest destruction in the tropics, the annual tree cover loss has steadily risen since the year 2000, reaching 12 million hectares in 2020 (WRI 2021). In the midst of the global climate crisis, tropical deforestation deterrence has integrated the agenda of countries and international agencies as a cheap and straightforward mean to reduce emissions.

In this context, remote sensing techniques, associated with adequate environmental policies, have been used to successfully reduce deforestation in several tropical countries. One of the best-known examples is the DETER system (Diniz et al. 2015), which helped to substantially reduce the deforestation rates in the Brazilian Amazonian biome (Assunção, Gandour, and Rocha 2019). From 2004 to 2012, deforestation figures decreased from 27,772 to 4,571 km^2, thanks, in part, to an effective land protection policy and a fine-tuned command-and-control strategy. Other initiatives have been successfully implemented in Peru (Weisse et al. 2019) and Indonesia (WRI 2021).

Until a few years ago, remote sensing-based systems aiming for near real-time (NRT) detection of forest disturbances were almost exclusively built using optical imagery as their main input data. However, persistent cloud cover can severely hamper optical observations (Hansen et al. 2016). Conversely, Synthetic Aperture Radar (SAR) data suffer from almost no deterioration in cloudy environments (except in the case of convective clouds, as pointed by Danklmayer et al. 2009). This constitutes a significant advantage in tropical regions which are cloudy year round (Ballère et al. 2021).

After the development of the pioneer JJ-FAST operational deforestation detection system, based on ALOS/PALSAR L-band sensor (Watanabe et al. 2018, 2021), several C-Band SAR-based operational or semi-operational systems have been recently implemented, using Sentinel-1A/B C-band sensors (Doblas et al. 2020; Mermoz et al. 2021; Reiche et al. 2021). In Brazil, the National Institute for Space Research (INPE) has implemented its own SAR-based detection system, DETER-R (Juan et al. 2022).

This work intends to study the performance of the four SAR-based forest disturbance systems operational over the tropics (CESBIO, INPE, JJ-FAST, RADD). We have established

and applied a benchmark framework, which enabled an objective comparison of the different methods, and to find the potential synergies among them.

2. Materials and methods

In this section, we will describe the different systems that were analysed and the benchmark framework built for their inter-comparison.

2.1. Forest disturbance data

During our study, we adapted, collected, combined, and compared the results of four different forest disturbance NRT detection systems, all of them based on the analysis of SAR time series, and of one forest disturbance detection system based on optical images, GLAD-S2. The detection procedure of the considered methods can be broken up into four main steps: 1) pre-processing of the input images, 2) pixel-wise analysis of the images, 3) flagging off the pixels that fall into the forest disturbance criteria, and 4) output of the analysis results, as raster or vector data.

All the analysed systems use a similar definition of forest disturbance, even if the used term sometimes changed to 'forest loss' or 'deforestation'. Our working definition of forest disturbance here is the partial or complete removal of forest cover on a area equivalent to the pixel size adopted by the system.

CESBIO/TropiSCO (Mermoz et al. 2021) computes the RCR (Radar Change Ratio) between the historic backscattering pre-processed SAR time series on a given pixel and the mean values of the last three acquisitions. The detection algorithm first flags the highest RCR values, which usually correspond to the radar shadow areas left after deforestation (Bouvet et al. 2018). After that, a lower threshold is used to extend the flagged area to the adjacent pixels that suffered alteration. This system is the only of the three tested high-resolution methods that does not use the Google Earth Engine (GEE, Gorelick et al. 2017) platform cloud-computing resources. Instead of that, the algorithm uses the computing power of the CNES-HPC (Centre National d'Études Spatiales High-Performance Computing) infrastructure to pre-process and analyse S1 time series. The maps based on the CESBIO's system are produced in the frame of the TropiSCO project (https://www.spaceclimateobservatory.org/tropisco-amazonia) and published on its own website (https://tropisco.org).

The RADD alerts (Reiche et al. 2021) are the result of long-term research of the Laboratory of Geoinformation Science and Remote Sensing of Wageningen University and Research (WUR) (Reiche et al. 2015, 2017, 2018; Vollrath, Mullissa, and Reiche 2020). Since 2021, RADD alerts are provided for most of the world's humid tropical forests. RADD alerts are publicly disseminated by the Global Forest Watch platform, which gathers users from different domains (local communities, academic departments, and global supply chains amongst others). The detection algorithm takes advantage of a sophisticated pre-processing chain (Mullissa et al. 2021), coupled with an anomaly-detection method based on Bayesian update theory. The warnings used in this study were produced by version 1.0 of the algorithm.

The INPE system (Juan et al. 2022) was developed as an operational outcome of the research described in Doblas et al. (2020). It uses the so-called Adaptative Linear Threshold (ALT) algorithm, which flags pixels where the SAR backscattering is lower than a certain value. This thresholding value is computed as a function of 1) the backscattering values of the

previous images, on the same location, and 2) the proximity of the analysed pixel with previously deforested areas. Unlike the other systems, INPE's was developed to supply field teams with fast and reliable forest loss information. Thus, INPE's operational products are originally tailored to minimize commission errors and to deliver lightweight vector data to the final users, instead of large-size raster outputs. For this study, we tested the INPE algorithm using two different parametrizations: the original, highly conservative parametrization, and a second one, which mimics the parameters of the RADD and CESBIO systems. This last version of the INPE system is hereby called INPE-HR.

JJ-FAST is developed by the Japanese Space Agency (JAXA). It is based on the analysis and thresholding of the L-Band ALOS/PALSAR-2 SAR satellite time series. Unlike the other analysed systems, JJ-FAST exploits the characteristics of both co-polarized and cross-polarized channels and their ratio (HH, HV, and HH/HV, respectively). Most of the warnings used in this study were computed using the 3.0 version of the detection algorithm, which is described in Watanabe et al. (2021).

The GLAD-S2 system was included here as a benchmark, as it uses optical images to detect forest disturbance. GLAD-S2 has been recently developed by the University of Maryland, as an upgrade of the long-time-running GLAD system, which made use of Landsat images. GLAD-S2 analyzes Sentinel-2 (S2) 10-m optical images to deliver alerts at higher spatial and temporal resolutions. Until the date of writing, no account of the system's accuracy has been published, whether by the authors or by independent researchers.

Table 1 summarizes the main characteristics of the analysed systems.

Table 1. Main characteristics of the analysed systems. SP: Spatio-temporal; MMU: minimum mapping unit; desc: descending orbits asc: ascending orbits.

System	Input images	Temporal Resolution	MMU (ha)	Processing Environment	Geographical Coverage
CESBIO	S1 Asc/Desc	6–12	0.1	Orfeo Toolbox	Guianas, Southeast Asia
INPE	S1 Desc	12	1	GEE	Brazilian Amazon
INPE-HR	S1 Desc	12	0.1	GEE	Brazilian Amazon
JJ-FAST	ALOS-PALSAR2	42	2.0	SigmaSAR	77 tropical countries
RADD	S1 Asc/Desc	6–12	0.1	GEE	44 Tropical countries
GLAD-S2	S2	5	0.1	GEE	Amazon basin

2.2. Combined systems

Additionally to the systems described above, we created three additional warning datasets, by merging the detection results of the three high-resolution SAR systems (CESBIO, INPE-HR and RADD) with the GLAD-S2 alerts. These new datasets are intended to simulate the results of three hypothetical combined optical-SAR warning systems, and will be called 'GLAD+CESBIO', 'GLAD+INPE-HR' and 'GLAD+RADD', respectively. The simulated results of every hypothetical system were obtained by performing a simple addition of the detections of the original methods.

2.3. Study sites and time frame

During this work, we analysed the forest disturbance data produced by the six systems we evaluated during the entire 2020 year.

The study was carried out in four areas in the Amazon basin, being three areas in Brazil and one area in the French Guiana-Suriname border region (Figure 1).

The Brazilian areas of interest (AOI) were named Acre, Munduruku and Calha Norte. The study area of Acre is located in the eastern Brazilian Amazon, with centre coordinates 8.179° S; 71.048° W. It has a total surface area of 56,892 km^2. In this study area, a typical fishbone deforestation pattern predominates, following the BR-364 major highway, which crosses the entire study area and gathers important population centres along it. This area has the highest percentage of deforestation among the studied areas (0.36% deforested in 2020). The Munduruku AOI is located in the central Brazilian Amazon at 7.281° S; 57.862° W and has a surface area of 44,033 km^2. In this region, the main driver of deforestation is illegal mining, which expands within protected areas, mainly the Munduruku indigenous territory, along the tributaries of the Tapajós River. The Calha Norte AOI is located at 0.948° S; 54261° W and has a total surface area of 43,942 km^2. Unevenly distributed fish-bone deforestation patterns predominate in this region. While the north of the AOI is well preserved, the south concentrates practically all the deforestation that takes place along the sides of the roads that connect the population centres to the left bank of the Amazon river.

In these three areas, the climate and rainfall are similar, with the rains concentrated in the months from November to March and the dry season from April to October. It is important to note that the deforestation that takes place along the roads, such as the fish-bone pattern, occurs mainly in the driest months, from May to September, when the opening of side roads in the forest is easier. Deforestation associated with illegal mining happens in the rainy season, as the dynamics of gold extraction that takes place along the streams need abundant water resources to happen.

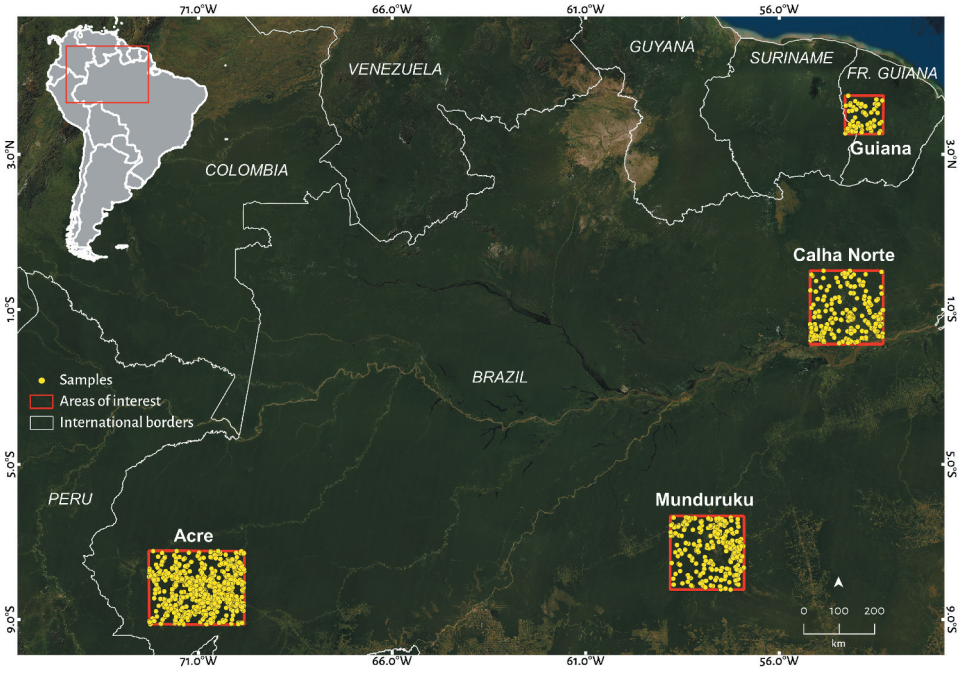

Figure 1. Location of the areas of interest and validation points.

The French Guiana and Suriname AOI is the most preserved among the four studied areas, with only 0.04% of total deforestation in 2020, relative to the forest baseline map. It is located at 4.021° N; 53.805° W and has a surface area of 12,027 km^2. The main driver of deforestation is the extraction of gold that takes place along the tributaries of the Lawa River that separates the two countries. The climate in this region presents a small difference in relation to the other three, as the rainy season takes place from December to July, with a small dry season in March. The main dry season runs from August to November.

Table 2 summarizes the main characteristics of the analysed areas.

Table 2. Main characteristics of the areas of interest (AOIs).

Area name	Code	Size (km^2)	Cloud cover	Main deforestation driver
Acre	AC	56,892	Moderate	Cattle Ranching, Soy
Munduruku	MDK	44,033	Moderate	Illegal mining
Calha norte	CN	43,942	High	Cattle ranching, selective logging
Guianas	GUI	12,027	Very High	Illegal mining

2.4. Forest/non-forest maps

An unbiased inter-comparison exercise of classification algorithms should ideally use the same forest/non-forest (F/NF) maps to determine the areas subject to detection. RADD and GLAD-S2 share the same F/NF maps that are readily available as GEE assets. They are composed of the improved forest baseline mask based on the primary humid tropical forest mask computed by Turubanova et al. (2018), minus the 2001–2019 forest loss areas, as computed by the University of Maryland's Global Land Analysis and Discovery team (https://glad.umd.edu/). Details on the GLAD forest loss methodology can be found in Hansen et al. (2013). CESBIO, INPE, and INPE-HR systems were customized to use the same input forest mask as GLAD-S2 and RADD, and ran over the same study areas.

2.5. Spatial accuracy assesment

Forest disturbance detection in tropical areas can be treated as a heavily unbalanced binary classification problem. In our case, the total amount of unchanged (i.e. intact forest) area during the studied period (2020) equals 96% of the total forest area, which confirms the unbalanced character of our problem. In such a case, a classic two-strata pixel-count validation methodology will fail to correctly evaluate detection accuracy. Even if we adopt an area-weighted strategy (Olofsson et al. 2013), the size differences between the intact and deforested sampling areas will distort the results. As pointed out by Olofsson et al. (2020), in these cases the omission errors tend to be heavily underestimated, as the chances to sample a missed disturbed patch are very low in the immensity of the intact forest stratum. The proposed solution relies on the creation of a third stratum, built as a buffer around the disturbed areas, which usually concentrates on omission errors. Accuracy metrics, in this case, will be computed following the inclusion probability concept proposed in Stehman (2014), adapted to our particular, multi-system case.

2.5.1. Reference sample design

We built a three-strata sampling space for each one of the high-resolution SAR systems used (CESBIO, INPE-HR and RADD), based on the forest disturbance map issued by every system. The strata were defined as follows:

- Deforested: Defined by the regions that suffered from forest disturbance during 2020, according to the corresponding NRT system.
- Intact buffer: This region is defined by a 200-m buffer around the Deforested sampling space, excluding the non-forested areas as defined by the initial F/NF map.
- Intact outside buffer: Defined as the remainder of the intact forest area, after subtraction of the disturbed and Intact buffer regions.

Once the sampling spaces were defined for every system, we randomly drew 498 points in each one of the sampling spaces. This sums up to 1494 samples that were distributed evenly among the three strata.

2.5.2. Reference labelling

The reference labelling tasks were accomplished using visual interpretation of Planetscope and Sentinel-2 monthly mosaics, made available within the Collect Earth platform (Saah et al. 2019). This platform allows for a streamlined interpretation and verification of the land cover changes using optical imagery. Additionally to the verification of forest disturbance on the given sample, monthly mosaics were used to date the land cover change, if any. The labelling was performed by one of the authors, who was not directly involved on the development of any of the analysed systems and assessed by the rest of the authors.

2.5.3. Agreement and confusion matrix definitions

During the agreement phase, the results of the reference visual labelling are compared to the disturbance maps issued by the analysed systems. During this phase, we noticed some minor but frequent misalignment between the different datasets and the validation Planet monthly basemaps made available by the Collect Earth platform. Most of the time, the misalignment was no bigger than the pixel size. To avoid unrealistic error estimations, especially over the buffered strata, we considered a 15-m tolerance during the agreement computation. This means that a sample labelled as 'deforested' will be correctly detected if the disturbance map issued by a given system has an active pixel on a 15-m buffer around the sample. Conversely, an intact sample will be assumed to be correctly detected by a given system if the corresponding disturbance map has an inactive pixel in a 15-m buffer around it.

In order to optimize the validation efforts, the points generated by random sampling of one system's strata were used to validate the other systems. This cross-validation methodology tends to reinforce and enrich the overall accuracy analysis results.

2.5.4. Spatial accuracy metrics

For every analysed system, we computed the F1-Score (F1), User's Accuracy (UA), and Producer's Accuracy (PA) taking the deforested class as the positive detection case. The F1-Score metric was adopted instead of the most common Overall Accuracy metric due to

the highly unbalanced character of the considered classes. The corresponding expressions were:

$$UA = p_{dd}/(p_{dd} + p_{df}) \tag{1}$$

$$PA = p_{dd}/(p_{dd} + p_{fd}) \tag{2}$$

$$F1 = 2 \cdot (UA \cdot PA)/(UA + PA) \tag{3}$$

where p_{dd} is the proportion of deforested area that was correctly mapped as deforested, p_{ff} the proportion of area that was correctly mapped as forest, p_{df} the proportion of intact area incorrectly mapped as deforested and p_{fd} the proportion of deforested area incorrectly mapped as forest.

Following the adopted protocol, we estimated p_{ij} as being:

$$\hat{p}_{ij} = W_i \frac{n_{ij}}{n_i} \tag{4}$$

where n_i is equal to the total samples belonging to the i strata, and n_{ij} the number of samples on this strata that belong to the j class (in our case, deforested or non-deforested) , and W_i is the proportion of area mapped as class i. In our case, where we used an additional buffered intact stratum to better quantify omissions, we will consider a third class b in 4 and then assimilate its results to the f class to compute the accuracy metrics F1, UA, and PA, following Stehman (2014).

2.6. Measuring performance on small patches

The adopted reference point sampling protocol considered the disturbed areas as a unique sampling space. While this protocol ensures statistical robustness, it may fail to measure the performance of the mapping algorithms in detecting forest changes on small patches, as they will be underrepresented in the corresponding sample subset. As the detection of this particular kind of disturbance can be of major importance in certain contexts, we decided to acquire an additional set of 150 points drawn from under 0.25 ha disturbed patches, as mapped by the three analysed systems whose minimum mapping unit is under 0.25 ha (CESBIO, RADD, INPE-HR). These points were used to perform accuracy computations, along with the points drawn from the non-altered strata.

2.7. Temporal benchmark

Timely forest disturbance alerts are a key aspect of deforestation-deterring initiatives, allowing enforcement agencies and local groups to counteract early degradation focuses. One of the main advantages of the SAR-based methodologies is considered to be its speed in frequently cloud-covered areas if compared to optical systems. In order to verify this point, we compared the detection date of the SAR-based systems with the GLAD-S2 system, which uses 5-day Sentinel-2 images.

It is worth pointing out that, for this particular comparison exercise to be fair, we need to define the detection delay as the time interval needed for a confirmed warning to be issued after the deforestation takes place, following every system premises. This issuing

can take several days, as the revisit frequency and the confirmation procedure vary from system to system.

- CESBIO: The RCR algorithm uses three S1 images (whether ascending or descending) to confirm a forest disturbance. We computed the delay time by multiplying by the S1 mean frequency map
- INPE: The system needs two preliminary warnings to confirm deforestation. As a mean, this usually takes 3.0 images to happen. As the system only uses S1 descending orbits, the delay can be bigger than CESBIO's.
- JJ-FAST: As noted in Watanabe et al. (2021), the system will issue the warnings 3–4 days after the 42-days observation period is finished.
- RADD: Based on Reiche et al. (2021), we deduced that the Bayesian update algorithm needs approximately 3.1 images to confirm an alert.
- GLAD-S2: Computing detecting delay for an optical alert system can be tricky, as it has a strong relationship with the cloud cover. Being so, we computed a warning delay map, based on the cloud cover over every GLAD-S2 warning issued on 2020 over our interest areas, to establish the detection delay as the delay between the first anomaly detection and the fourth cloud-free S2 observation of the pixel (GLAD-S2 assumes a warning as confirmed after the fourth observation of an anomaly).

Once established the detection delays for every warning map of every system, we use simple map algebra to compute the issuing time and the time differences among the systems. After that we computed the difference statistics for every map and every AOI, taking GLAD-S2 as a reference.

3. Results

3.1. Forest disturbance maps

As expected, the forest disturbance maps produced by the high-resolution SAR-based systems were quite similar, with the main differences being located on the edges of the deforested regions. The INPE and JJ-FAST systems, as per their design specifications, missed most of the smaller deforested patches, while the RADD system seemed to be more precise in these cases. Figure 2 presents some of the results on deforestation detection over the four analysed areas.

It is worth noting that two of the systems (CESBIO and INPE) were modified to run under the same premises (i.e. Forest/Non-Forest mask) as the global systems (GLAD-S2 and RADD). Table 3 summarizes the total deforested area found by the analysed systems over the four AOIs. In all the considered regions, the area mapped as deforested is several orders of magnitude smaller than the intact forested area. This kind of class unbalance results are expected and frequent in deforestation studies on tropical regions. In this study, we adopted specific evaluation techniques suited to this kind of situation, such as buffered sampling spaces and F1-Score metrics.

After the classification maps were computed, the reference points were drawn over them. A small fraction of the reference points were discarded by the interpreter due to

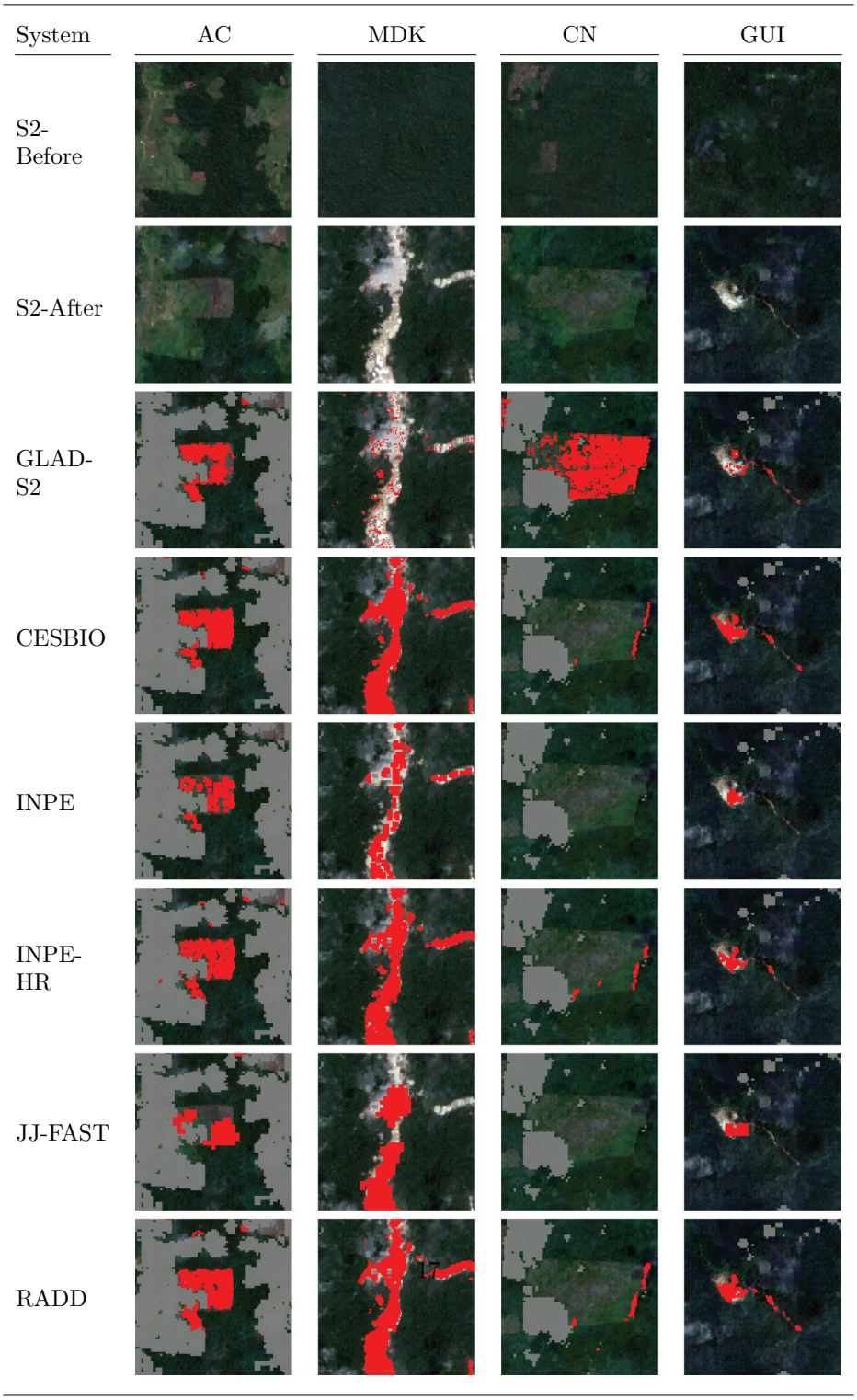

Figure 2. 2-km wide thumbnails of the detection results, captured on example locations on each of the tested areas. S2-Before: 2019 dry season Sentinel true-color image mosaic. S2-After: 1st quarter

Table 3. Areas of the disturbed (D) and intact forest (F) maps produced by every system, as a function of the study area. Area units are km^2. AC: Acre; CN: Calha Norte; GUI: French Guiana; MDK: Munduruku.

System	AC		MDK		CN		GUI		Total	
	D	F	D	F	D	F	D	F	D	F
CESBIO	176.7	51960	34.5	40311	34.0	32737	4.2	11738	249.4	136745
INPE	76.9	52059	18.1	40327	22.2	32749	0.9	11741	118.1	136877
INPE-HR	206.1	51930	47.6	40298	54.7	32716	5.1	11737	313.6	136681
JJ-FAST	229.2	51907	81.0	40264	30.6	32740	0.8	11742	341.7	136653
RADD	209.5	51927	55.0	40290	47.7	32723	7.6	11735	319.8	136675
GLAD-S2	166.5	51970	39.0	40306	54.3	32717	2.0	11740	261.8	136733

their ambiguous nature (it was not clear whether they were deforested or not). The final distribution of the reference points is summarized in Table 4.

Table 4. Final number of samples used in the validation phase, enumerated as a function of the sampling stratum and the map used on the sample space design.

Sampling space	CESBIO	INPE-HR	RADD	Total
Deforestation	163	165	166	494
Deforestation on small ($\leq$ 0.25 ha) patches	50	50	50	150
Intact forest within deforestation buffer	168	166	165	499
Intact forest outside deforestation buffer	167	167	167	501
Total	548	548	548	1644

3.2. Spatial accuracy

Once the reference points were labelled, we computed the corresponding accuracy metrics following the equations presented above. Figures 3 and 4 summarize the results of the validation procedure, in terms of spatial accuracy metrics. All the figures and tables below include the evaluation of the performance of the hybrid systems, which were obtained by the combination of radar and optical systems.

Tables 5 and 6 reflect the results of the validation procedure, in term of pixel-count and in terms of area-weighted probabilities (Olofsson et al. 2013).

The obtained accuracy metrics point to the homogeneous performance of the three high-resolution Sentinel-1-based systems (CESBIO, RADD and INPE-HR). Sentinel-2-based GLAD-S2 systems have similar performance. If measured using sample-count metrics, SAR systems show better performance. Area-based metrics show comparable results across all four systems. The performance of the hybrid systems (which combine the alerts of optical and SAR-based systems) was always superior to the performance of the original systems.

Tables 7 and 8 summarize the results of the validation procedure, using only deforestation samples coming from very small (smaller than 0.25 ha) patches.

2021 true color mosaic. In the detection thumbnails, the detected deforestation areas are represented in red. The non-forest areas are masked in grey. S2 images were masked using the S2/CLOUDLESS cloud probability data. The AC (Acre) example shows a classic pasture-related deforestation pattern. MDK (Munduruku) shows a large 'garimpo' (illegal mining) pit growing inside an indigenous land. The CN (Calha Norte) example is a slash-but-not-burned deforested area. Finally, the GUI (Guiane) example shows a tiny, difficult-to-spot network of illegal mining pits.

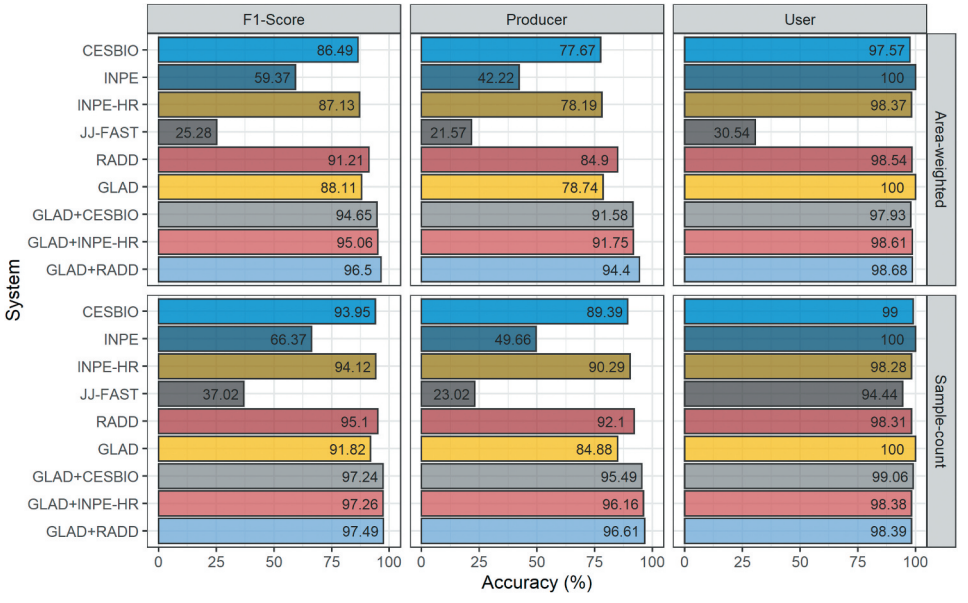

Figure 3. Graphical depiction of the accuracy comparison results. Results using the original sample set.

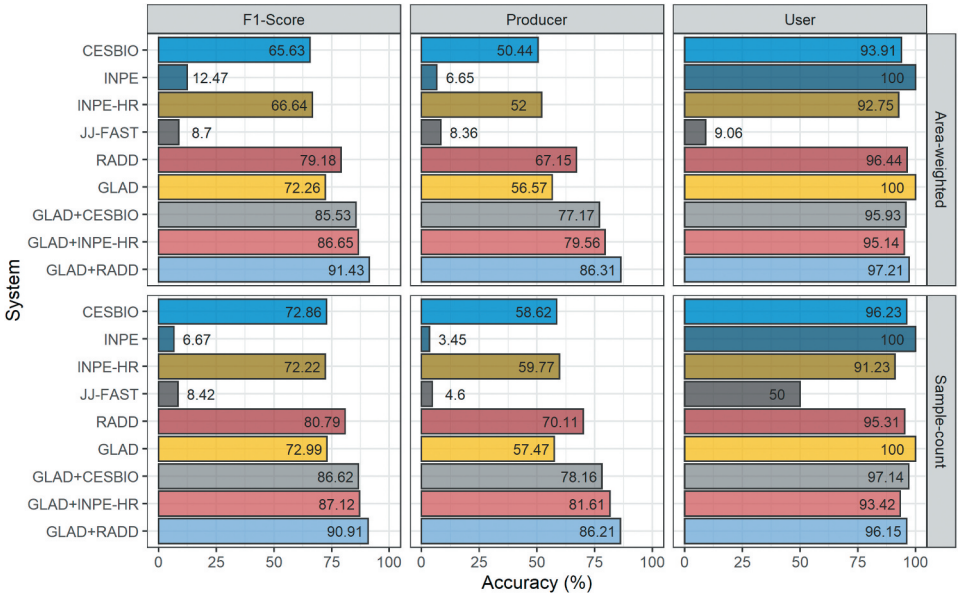

Figure 4. Graphical depiction of the accuracy comparison results. Results using only deforestation samples coming from small (< 0.25 ha) deforested patches.

3.3. Temporal accuracy

As explained above, after computing the delay associated with the detections of every system on a pixel-wise basis, we applied a map algebra procedure to compute the relative detection delays of the analysed systems, taking the GLAD-S2 system as a reference. The comparison

Table 5. Pixel-count accuracy results, general survey. TP: True positives; FP: False positives; FN: False negatives; TN: True negatives; OA: Overall accuracy; UA: User's accuracy; PA: Producer's accuracy. The results do not include the additional small deforestation samples. *: Hypothetical system.

System	N_{TP}	N_{FP}	N_{FN}	N_{TN}	F1	UA	PA
CESBIO	396	4	47	1047	93.95	99.00	89.39
GLAD-S2	376	0	67	1051	91.82	100.00	84.88
INPE	220	0	223	1051	66.37	100.00	49.66
INPE-HR	400	7	43	1044	94.12	98.28	90.29
JJ-FAST	102	6	341	1045	37.02	94.44	23.02
RADD	408	7	35	1044	95.10	98.31	92.10
*GLAD+CESBIO	423	4	20	1047	97.24	99.06	95.49
*GLAD+INPE-HR	426	7	17	1044	97.26	98.38	96.16
*GLAD+RADD	428	7	15	1044	97.49	98.39	96.61

Table 6. Area-weighted results, general survey. TP: True positives; FP: False positives; FN: False negatives; TN: True negatives; OA: Overall accuracy; UA: User's accuracy; PA: Producer's accuracy. The results do not include the additional small deforestation samples. *: Hypothetical system.

System	p_{TP}	p_{FP}	p_{FN}	p_{TN}	F1	UA	PA
CESBIO	0.33	0.01	0.10	99.56	86.49	97.57	77.67
GLAD-S2	0.34	0.00	0.09	99.57	88.11	100.00	78.74
INPE	0.18	0.00	0.25	99.57	59.37	100.00	42.22
INPE-HR	0.34	0.01	0.09	99.56	87.13	98.37	78.19
JJ-FAST	0.09	0.21	0.34	99.36	25.28	30.54	21.57
RADD	0.36	0.01	0.06	99.56	91.21	98.54	84.90
*GLAD+CESBIO	0.39	0.01	0.04	99.56	94.65	97.93	91.58
*GLAD+INPE-HR	0.39	0.01	0.04	99.56	95.06	98.61	91.75
*GLAD+RADD	0.40	0.01	0.02	99.56	96.50	98.68	94.40

Table 7. Pixel-count accuracy results, using only deforestation samples belonging to small (smaller than 0.25 ha) patches. TP: True positives; FP: False positives; FN: False negatives; TN: True negatives; OA: Overall accuracy; UA: User's accuracy; PA: Producer's accuracy. *: Hypothetical system.

System	N_{TP}	N_{FP}	N_{FN}	N_{TN}	F1	UA	PA
CESBIO	51	2	36	1095	72.86	96.23	58.62
GLAD-S2	50	0	37	1097	72.99	100.00	57.47
INPE	3	0	84	1097	6.67	100.00	3.45
INPE-HR	52	5	35	1092	72.22	91.23	59.77
JJ-FAST	4	4	83	1093	8.42	50.00	4.60
RADD	61	3	26	1094	80.79	95.31	70.11
*GLAD+CESBIO	68	2	19	1095	86.62	97.14	78.16
*GLAD+INPE-HR	71	5	16	1092	87.12	93.42	81.61
*GLAD+RADD	75	3	12	1094	90.91	96.15	86.21

only takes place on the areas where both compared deforestation maps are superimposed. Table 9 summarizes the outcomes of the relative warning delay computation.

Detection delay results show how cloudier areas, such as Guyana (GUY), have faster detections coming from SAR systems. In areas with less cloud cover, such as the Calha Norte (CN) area, optical detections were faster. The three high-resolution Sentinel-1 based system have similar performances, RADD being marginally faster in most of the analysed regions (Figure 5).

Table 8. Area-weighted results, using only deforestation samples belonging to small (smaller than 0.25 ha) patches. TP: True positives; FP: False positives; FN: False negatives; TN: True negatives; OA: Overall accuracy; UA: User's accuracy; PA: Producer's accuracy. *: Hypothetical system.

System	p_{TP}	p_{FP}	p_{FN}	p_{TN}	F1	UA	PA
CESBIO	0.13	0.01	0.12	99.74	65.63	93.91	50.44
GLAD-S2	0.14	0.00	0.11	99.75	72.26	100.00	56.57
INPE	0.02	0.00	0.23	99.75	12.47	100.00	6.65
INPE-HR	0.13	0.01	0.12	99.74	66.64	92.75	52.00
JJ-FAST	0.02	0.21	0.23	99.54	8.70	9.06	8.36
RADD	0.17	0.01	0.08	99.74	79.18	96.44	67.15
*GLAD+CESBIO	0.19	0.01	0.06	99.74	85.53	95.93	77.17
*GLAD+INPE-HR	0.20	0.01	0.05	99.74	86.65	95.14	79.56
*GLAD+RADD	0.21	0.01	0.03	99.74	91.43	97.21	86.31

Table 9. Relative deforestation detection times for the analysed systems, expressed as days after (positive) or before (negative). Values expressed as mean ± standard error. AC: Acre; CN: Calha Norte; GUI: French Guiana; MDK: Munduruku.

System	CN	AC	MDK	GUI
CESBIO	32.2 ± 0.11	−11.4 ± 0.04	8.8 ± 0.92	−41.4 ± 0.52
INPE-HR	33.1 ± 0.1	0.5 ± 0.44	7.4 ± 0.09	−4.4 ± 0.64
INPE	62.9 ± 0.13	24.4 ± 0.05	52.2 ± 1.56	32.9 ± 1.23
JJ-FAST	80.95 ± 0.25	41.74 ± 0.09	31.11 ± 0.31	−9.14 ± 2.03
RADD	32.4 ± 0.1	−12.9 ± 0.03	−2.3 ± 0.93	−41 ± 0.53

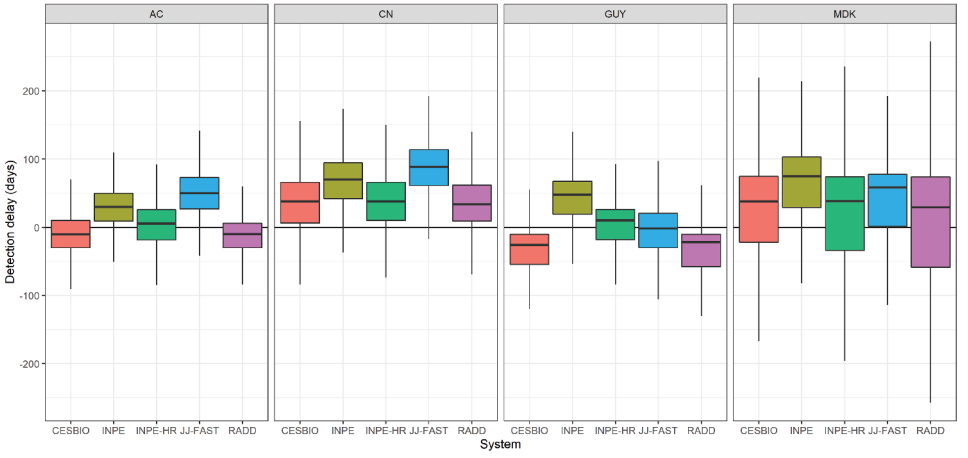

Figure 5. Detection delays, as compared with the reference optical state-of-the-art forest disturbance detection system (GLAD-S2), over the four studied regions. AC: Acre; CN: Calha Norte; GUI: French Guiana; MDK: Munduruku. Negative values implies that the corresponding system detected disturbance before the optical one.

4. Discussion

Forest disturbance results of the tested algorithms affirm that all the SAR-based high-resolution systems (CESBIO, INPE-HR and RADD) yield similar results, with sample-count-based F1 scores higher than 94%. This affirms the robustness of C-band time series as a forest disturbance indicator, regardless of the methodological approach to the time series analysis.

The systematic and rigorously applied validation protocol confirms the visual impression, as the three high-resolution systems reached high accuracy levels, which are comparable to the reference, state-of-the-art optical system (GLAD-S2). User accuracies of both GLAD-S2 and INPE methods are remarkable: no false positives were found. This was expected for the INPE system, as it was specifically designed for, but it was surprising for the more general-purpose GLAD-S2 system.

The results show how coarse-resolution methods (INPE and JJ-FAST) have their performance severely degraded on small-deforestation scenarios, while other systems using smaller scales are able to maintain high accuracy levels. The RADD system excels in this kind of situation, having a F1-Score well above the other tested systems. Hybrid systems also have better performances than the original systems.

All C-band backscattering-based SAR systems show a known flaw in areas that did not undergo complete vegetation removal during the deforestation process. The non-photosynthetic remnants of vegetation produced by an initial deforestation process will have a characteristic spectral signature, whilst their backscattering properties for short-wavelength SAR will not change significantly. SAR detection will occur after the burning, or mechanical clearing, of the slashed vegetation. CESBIO's methodology, which uses the SAR shadowing effects to locate deforested areas and then applies a lower threshold to flag the remainder of the disturbed area, has been shown to overcome this problem in many areas (Bouvet et al. 2018), but it can still produce some omissions common to other SAR systems, such as a the one illustrated in the images of Figure 2, column 'CN'.

JJ-FAST presents interesting results, being a pioneering method that uses a coarser resolution sensor. However, both user's and producer's accuracies are much smaller than the ones produced by Sentinel-1-based methods. Image resolution (50 vs. 10 m) and bigger minimum mapping unit (2 ha vs. 0.1 ha) explain the differences in the producer's accuracy, as many smaller disturbed patches were not detected. The low values of user's accuracy can be associated with two main reasons: 1) the 'pixelation' effect, due to the 50-m resolution of the method, that can extend warning polygons beyond the real disturbed area and 2) the shifting of the threshold values on certain areas, as introduced on the third version of the algorithm, seems to introduce a great quantity of new, false positive-prone warnings (see Figure 6)

The three tested hypothetical systems, which were conceived as an exercise to investigate the potential performance of a combined optical-radar warning system, excelled in the producer's accuracy, as shown in Figure 3, at the cost of a slight decrease on the user's accuracy, if compared with GLAD-S2. This means that a combined system will be able to detect more deforested areas, especially on tiny patches, but will still produce false warnings, at similar levels as the studied SAR systems.

Although GLAD-S2 shows excellent accuracy results, some issues should be raised, mostly related to cloud cover. S2 cloud masking is an ongoing research subject, and several cloud masking systems have been developed to deal with this non-trivial problem (Skakun et al. 2022). Some of these systems imply high-cost computations, others can be applied in real time. GLAD-S2 cloud masking is based on the cloud probability data computed during the image processing and is able to deliver results on a near real-time framework. Although generally this algorithm shows good results, it fails to distinguish clouds from very bright, non-cloudy pixels, such as those related to open-pit mining. This issue boosts GLAD-S2 omissions in illegal mining areas, such as the one illustrated in

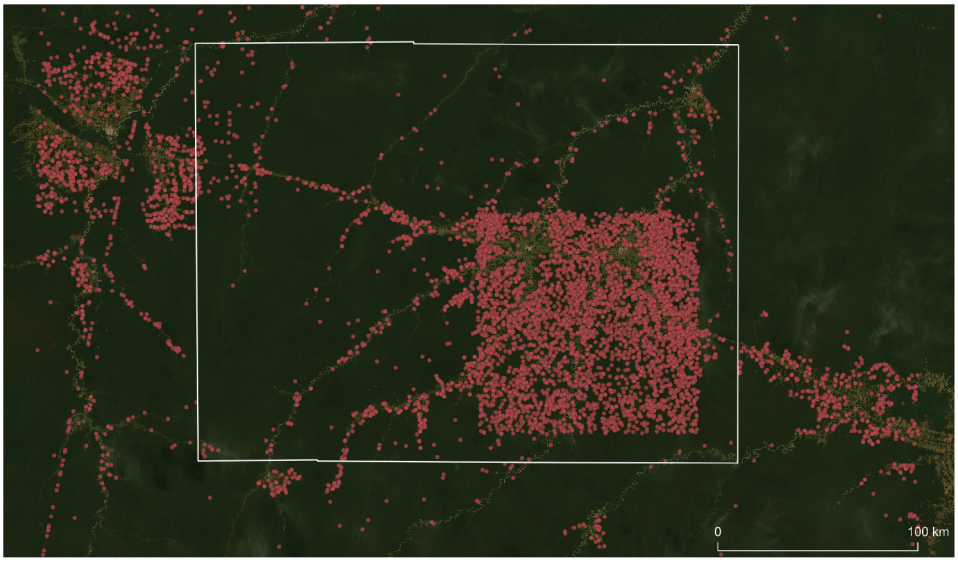

Figure 6. JJ-FAST system detection warnings on the Acre area (in white), represented here as red points centered on every warning polygon. Notice the densification of alerts derived from the use of different detection parameters the SE regions of the interest area.

Figure 2, columns 'MDK' and 'GUI', and can explain the Producer's accuracy results, with omissions that range between 15 and 20%.

The study of the delay of warning issuing highlights the importance of SAR systems in areas with a persistent cloud cover. In the Guianas AOI, all the high-resolution SAR systems were faster than the reference optical system. CESBIO and RADD took advantage of the frequent coverage of this area by the Sentinel-1 constellation, issuing alerts 41 days before their optical counterpart. INPE-HR system temporal advantage was lower (4 days), due to the fact that this system does not ingest the S1 ascending orbit data available in the Guianas. The results of the remainder of the AOI showed that the SAR temporal advantage reduces in areas with lower cloud coverage, but still prevails for the RADD system in two out of three areas.

5. Conclusions

Our work intended to compare the SAR-based forest disturbance NRT detection systems operational nowadays against a state-of-the-art optical system, by applying a robust testing protocol. We sampled and examined a total of 1644 locations in 4 different areas in Brazil and the Guianas to validate every system's performance. We also computed the detection timing, in order to determine the delay of response to disturbance.

The adopted validation protocol, which included many samples near the border of the detected deforested areas and in small deforested patches, was conceived as a kind of 'stress test' that should reveal the performance of every system in the most error-prone areas.

The results show an excellent performance of the SAR systems based on Sentinel-1 sensor data, which outperformed the reference optical system on total accuracy and

producer's accuracy. The reference optical system showed better performance on the user's accuracy, showing no false positives on the general testing scenario.

The results affirm that an integrated approach to forest disturbance detection, merging the products delivered by optical and SAR-based systems can overcome the results of the individual systems, with a slight increase in commission errors. This approach, which has been recommended by several authors (see for example Reiche et al. 2016), can establish a new state-of-the-art on tropical forest near real-time deforestation detection.

Although meaningful, these results should be taken with precaution if applied outside the Amazonian basin. In this case, a new comparison exercise will be advisable.

Acknowledgments

PlanetScope data used on validation was provided through Norway's International Climate and Forests Initiative (NICFI). Contains modified Copernicus Sentinel data (2021).

Disclosure statement

J.D.,S.M.,A.B.,J.R. and M.W. participate or have participated on the development of the analysed systems and hereby declare that they have not, in any way, influenced the validation process, which has been performed by L.L.

Funding

The first author was funded by the National Council for Scientific and Technological Development, project "Monitoring Brazilian Biomes by Satellite – Building new capacities"/process 444418/2018-0, grant #350303/2021-5, and the Coordenação de Aperfeiçoamento de Pessoal de Nível Superior - Brasil (CAPES) - Finance Code 001, as part of the Internationalization program PrInt-INPE. RADD project received funding through Norway's Climate and Forest Initiative (NICFI), the US Government's SilvaCarbon program.

ORCID

Juan Doblas Prieto http://orcid.org/0000-0002-2573-3783
Alexandre Bouvet http://orcid.org/0000-0002-7428-4339

Data availability statement

The data that support the findings of this study are available from the corresponding author, J.D., upon reasonable request.

References

Assunção, J., C. Gandour, and R. Rocha. 2019. "Deterring Deforestation in the Amazon: Environmental Monitoring and Law Enforcement." *Climate Policy Initiative Report*.

Ballère, M., A. Bouvet, S. Mermoz, T. Le Toan, T. Koleck, C. Bedeau, M. André, E. Forestier, P. L. Frison, and C. Lardeux. 2021. "SAR Data for Tropical Forest Disturbance Alerts in French Guiana: Benefit Over Optical Imagery." *Remote Sensing of Environment* 252: 112159. doi:10.1016/j.rse.2020.112159.

Bouvet, A., S. Mermoz, M. Ballère, T. Koleck, and T. Le Toan. 2018. "Use of the SAR Shadowing Effect for Deforestation Detection with Sentinel-1 Time Series." *Remote Sensing* 10 (8): 1250. doi:10.3390/rs10081250.

Danklmayer, A., B. R. J. Doring, M. Schwerdt, and M. Chandra. 2009. "Assessment of Atmospheric Propagation Effects in SAR Images." *IEEE Transactions on Geoscience and Remote Sensing : A Publication of the IEEE Geoscience and Remote Sensing Society* 47 (10): 3507–3518. doi:10.1109/TGRS.2009.2022271.

Diniz, C. G., A. Antonio De Almeida Souza, D. Correa Santos, M. Correa Dias, N. Cavalcante Da Luz, D. Rafael Vidal De Moraes, J. Sant Ana Maia, et al. 2015. "DETER-B: The New Amazon Near Real-Time Deforestation Detection System." *IEEE Journal of Selected Topics in Applied Earth Observations and Remote Sensing* 8 (7): 3619–3628. doi:10.1109/JSTARS.2015.2437075.

Doblas, J., Y. Shimabukuro, S. Sant'Anna, A. Carneiro, L. Aragão, and C. Almeida. 2020. "Optimizing Near Real-Time Detection of Deforestation on Tropical Rainforests Using Sentinel-1 Data." *Remote Sensing* 12 (23): 1–31. doi:10.3390/rs12233922.

Gorelick, N., M. Hancher, M. Dixon, S. Ilyushchenko, D. Thau, and R. Moore. 2017. "Google Earth Engine: Planetary-Scale Geospatial Analysis for Everyone." *Remote Sensing of Environment* 202: 18–27. Big Remotely Sensed Data: tools, applications and experiences. doi:10.1016/j.rse.2017.06.031.

Hansen, M. C., A. Krylov, A. Tyukavina, P. V. Potapov, S. Turubanova, B. Zutta, S. Ifo, B. Margono, F. Stolle, and R. Moore. 2016. "Humid Tropical Forest Disturbance Alerts Using Landsat Data." *Environmental Research Letters* 11 (3): 34008. doi:10.1088/1748-9326/11/3/034008.

Hansen, M. C., P. V. Potapov, R. Moore, M. Hancher, S. A. Turubanova, A. Tyukavina, D. Thau, et al. 2013. "High-Resolution Global Maps of 21st-Century Forest Cover Change." *Science* 80 (342): 850–853. doi:10.1126/science.1244693.

Harris, N. L., D. A. Gibbs, A. Baccini, R. A. Birdsey, S. de Bruin, M. Farina, L. Fatoyinbo, et al. 2021. "Global Maps of Twenty-First Century Forest Carbon Fluxes." *Nature Climate Change* 11 (3): 234–240. doi:10.1038/s41558-020-00976-6.

Juan, D., M. S. Reis, A. P. Belluzzo, C. B. Quadros, R. V. M. Douglas, C. A. Almeida, E. P. M. Luis, A. F. A. Carvalho, J. S. S. Sidnei, and Y. E. Shimabukuro. 2022. "DETER-R: An Operational Near-Real Time Tropical Forest Disturbance Warning System Based on Sentinel-1 Time Series Analysis." *Remote Sensing* 14: 15. doi:10.3390/rs14153658.

Mermoz, S., A. Bouvet, T. Koleck, M. Ballère, and T. Le Toan. 2021. "Continuous Detection of Forest Loss in Vietnam, Laos, and Cambodia Using Sentinel-1 Data." *Remote Sensing* 13: 23. doi:10.3390/rs13234877.

Mullissa, A., A. Vollrath, C. Odongo-Braun, B. Slagter, J. Balling, Y. Gou, N. Gorelick, and J. Reiche. 2021. "Sentinel-1 Sar Backscatter Analysis Ready Data Preparation in Google Earth Engine." *Remote Sensing* 13 (10): 5–11. doi:10.3390/rs13101954.

Olofsson, P., P. Arévalo, A. B. Espejo, C. Green, E. Lindquist, R. E. McRoberts, and M. J. Sanz. 2020. "Mitigating the Effects of Omission Errors on Area and Area Change Estimates." *Remote Sensing of Environment* 236 (October 2019): 111492. doi:10.1016/j.rse.2019.111492.

Olofsson, P., G. M. Foody, S. V. Stehman, and C. E. Woodcock. 2013. "Making Better Use of Accuracy Data in Land Change Studies: Estimating Accuracy and Area and Quantifying Uncertainty Using Stratified Estimation." *Remote Sensing of Environment* 129: 122–131. doi:10.1016/j.rse.2012.10.031.

Reiche, J., S. de Bruin, D. Hoekman, J. Verbesselt, and M. Herold. 2015. "A Bayesian Approach to Combine Landsat and ALOS PALSAR Time Series for Near Real-Time Deforestation Detection." *Remote Sensing* 7 (5): 4973–4996. doi:10.3390/rs70504973.

Reiche, J., E. Hamunyela, J. Verbesselt, D. Hoekman, and M. Herold. 2017. "Improving Near-Real Time Deforestation Monitoring in Tropical Dry Forests by Combining Dense Sentinel-1 Time Series with Landsat and ALOS-2 PALSAR-2." *Remote Sensing of Environment* 204 (April): 147–161. doi:10.1016/j.rse.2017.10.034.

Reiche, J., R. Lucas, A. L. Mitchell, J. Verbesselt, D. H. Hoekman, J. Haarpaintner, J. M. Kellndorfer, et al. 2016. "Combining Satellite Data for Better Tropical Forest Monitoring." *Nature Climate Change* 6 (2): 120–122. doi:10.1038/nclimate2919.

Reiche, J., A. Mullissa, B. Slagter, Y. Gou, N. Erdene Tsendbazar, C. Odongo-Braun, A. Vollrath, et al. 2021. "Forest Disturbance Alerts for the Congo Basin Using Sentinel-1." *Environmental Research Letters* 16 (2): 24005. doi:10.1088/1748-9326/abd0a8.

Reiche, J., R. Verhoeven, J. Verbesselt, E. Hamunyela, N. Wielaard, and M. Herold. 2018. "Characterizing Tropical Forest Cover Loss Using Dense Sentinel-1 Data and Active Fire Alerts." *Remote Sensing* 10 (5): 1–18. doi:10.3390/rs10050777.

Saah, D., G. Johnson, B. Ashmall, G. Tondapu, K. Tenneson, M. Patterson, A. Poortinga, et al. 2019. "Collect Earth: An Online Tool for Systematic Reference Data Collection in Land Cover and Use Applications." *Environmental Modelling & Software* 118: 166–171. doi:10.1016/j.envsoft.2019.05.004.

Skakun, S., J. Wevers, C. Brockmann, G. Doxani, M. Aleksandrov, M. Batič, D. Frantz, et al. 2022. "Cloud Mask Intercomparison eXercise (CMIX): An Evaluation of Cloud Masking Algorithms for Landsat 8 and Sentinel-2." *Remote Sensing of Environment* 274: 112990. doi:10.1016/j.rse.2022.112990.

Stehman, S. V. 2014. "Estimating Area and Map Accuracy for Stratified Random Sampling When the Strata are Different from the Map Classes." *International Journal of Remote Sensing* 35 (13): 4923–4939. doi:10.1080/01431161.2014.930207.

Turubanova, S., P. V. Potapov, A. Tyukavina, and M. C. Hansen. 2018. "Ongoing Primary Forest Loss in Brazil, Democratic Republic of the Congo, and Indonesia." *Environmental Research Letters* 13 (7): 2000–2010. doi:10.1088/1748-9326/aacd1c.

Vollrath, A., A. Mullissa, and J. Reiche. 2020. "Angular-Based Radiometric Slope Correction for Sentinel-1 on Google Earth Engine." *Remote Sensing* 12 (11): 1–14. doi:10.3390/rs12111867.

Watanabe, M., C. N. Koyama, M. Hayashi, I. Nagatani, and M. Shimada. 2018. "Early-Stage Deforestation Detection in the Tropics with L-Band SAR." *IEEE Journal of Selected Topics in Applied Earth Observations and Remote Sensing* 11 (6): 2127–2133. doi:10.1109/JSTARS.2018.2810857.

Watanabe, M., C. N. Koyama, M. Hayashi, I. Nagatani, T. Tadono, and M. Shimada. 2021. "Refined Algorithm for Forest Early Warning System with ALOS-2/PALSAR-2 ScanSar Data in Tropical Forest Regions." *Remote Sensing of Environment* 265 (November 2020): 112643. doi:10.1016/j.rse.2021.112643.

Weisse, M. J., R. Noguerón, R. Eduardo, V. Vicencio, and D. Arturo Castillo Soto. 2019. "Use of Near-Real-Time Deforestation Alerts: A Case Study from Peru." *Technical Report*. Washington, DC: WRI.ORG. https://www.wri.org/publication/use-near-real-time-deforestation-alerts

WRI. 2021. "Global Forest Review." Washington, DC. Accessed 2022 February 21. https://research.wri.org/gfr/forest-pulse